

# Phonon Directionality Determines the Polarization of the Band-Edge Exciton Emission in Two- Dimensional Metal Halide Perovskites

*Roman Krahné<sup>1</sup>, Alexander Schleusener<sup>1</sup>, Mehrdad Faraji<sup>1,2</sup>, Lin-Han Li<sup>3,4</sup>, Miao-Ling Lin<sup>3,4</sup>, and Ping-Heng Tan<sup>3,4</sup>.*

<sup>1</sup>Optoelectronics Research Unit, Istituto Italiano di Tecnologia (IIT), Via Morego 30, 16163 Genoa, Italy

<sup>2</sup>Dipartimento di Chimica e Chimica Industriale, Università degli Studi di Genova, Via Dodecaneso, 31, 16146 Genova, Italy

<sup>3</sup>State Key Laboratory of Superlattices and Microstructures, Institute of Semiconductors, Chinese Academy of Sciences, 100083 Beijing, China

<sup>4</sup>Center of Materials Science and Optoelectronics Engineering & CAS Center of Excellence in Topological Quantum Computation, University of Chinese Academy of Sciences, 100049 Beijing, China.

Keywords: two-dimensional perovskite, excitons, phonons, photoluminescence, Raman spectroscopy

Two-dimensional metal-halide perovskites are highly versatile for light-driven applications due to their exceptional variety in material composition, which can be exploited for tunability of mechanical and optoelectronic properties. The band edge emission is governed by the exciton fine structure that is defined by structure and composition of both organic and inorganic layers. Moreover, electronic and elastic properties are intricately connected in these materials. Electron-phonon coupling plays a crucial role in the recombination dynamics. However, the nature of the electron-phonon coupling, as well as which kind of phonons are involved, is still under debate. Here we investigate the emission and phonon response from single two-dimensional lead-iodide microcrystals with angle-resolved polarized spectroscopy. We find an intricate dependence of the emission polarization with the vibrational directionality in the materials, which clearly reveals that several bands of the low-frequency phonons of the inorganic lead-iodide perovskite lattice play the key role in the band edge emission. Our findings demonstrate how the emission spectrum and polarization of two-dimensional layered perovskites can be designed by their material composition, which is essential for optoelectronic applications, where fine control on the spectral and structural properties of the light is desired.

Two-dimensional layered organic-inorganic perovskites alternate sub-nanometer thin semiconductor layers consisting of a single plane of inorganic metal halide octahedra with dielectric layers formed by the organic cations.<sup>1</sup> This leads to strong confinement of the electronic

carriers, which renders such systems as natural quantum wells, with binding energies for electron-hole pairs (excitons) of the order of several hundred meV.<sup>2-5</sup> These properties are highly appealing for light emission and manipulation in a large variety of applications, in particular, because the emission can be tailored by the choice of the halide, and to some extent by the composition of the organic layers that influence the structural and electrical properties of the material.<sup>6-8</sup> Here the static distortions induced by the binding of the organic cations to the octahedra layer have a significant impact on the crystal structure and electron-phonon coupling.<sup>6</sup> Furthermore the organic layer defines the dielectric confinement of the charge carriers in the semiconductor metal halide lattice. Several recent works investigated the confinement effects on the exciton fine structure, and on the dark singlet and a bright triplet states at the band edge,<sup>9-13</sup> and provided a detailed understanding with insights on crystal symmetry, polar distortions, and other structural property effects.<sup>11, 12, 14-18</sup> However, the influence of the electron-phonon coupling in the recombination dynamics is much less investigated, and which mechanisms and phonon bands contribute to the band edge emission is under debate. For example, a series of equally spaced peaks in the emission spectra has been attributed to a vibronic progression due to coupling to phonons of the organic cations<sup>19-21</sup>, while other works observed emission dynamics that were related to polaron formation.<sup>22-25</sup>

In this work, we correlate the band-edge exciton emission of single two-dimensional lead-iodide perovskite flakes with their phonon response. The latter is measured by Raman spectroscopy under resonant (above band gap) and non-resonant (below band gap) excitation. In detail, we record angle-resolved polarized photoluminescence (PL) and Raman spectra from the same region of single, regularly shaped 2D microcrystals, where we resolve emission peaks with width of less than 0.5 meV, and where we have access to the low-frequency Raman response down to 8 cm<sup>-1</sup>

(equivalent to 1 meV). This allows to directly correlate the in-plane polarization of the different exciton emission bands with the directionality of the phonon modes of the inorganic octahedra lattice. We find a distinct polarization of the different emission peaks that is strongly connected to the directionality of the low-frequency phonon bands. Furthermore, these optical properties critically depend on the type of organic cation in the 2D crystal.

## RESULTS & DISCUSSION

**Figure 1 (A-B)** illustrates the main features of the optical setup that enables angle-resolved PL and Raman spectroscopy on the same region of a single micron-sized crystal. The coaxial beam path of the different laser lines allows to measure under excitation with different wavelengths (457 nm for above, and 633 nm for below band gap excitation), and the switching of the grating in the spectrometer enables to record PL and Raman spectra from the same excitation spot. In the experiments, we first recorded the PL that required much shorter integration time (fractions of a second) and less excitation power, and then the Raman signal that was integrated over several tens of seconds and, if needed, measured with higher excitation power. In all cases we assured that the beam exposure did not lead to degradation or damage of the sample.

As metal halide perovskite samples, we chose two-dimensional lead-iodide crystals in the Ruddlesden-Popper phase with butylammonium (BA), undecylammonium (UDA), and phenylethylammonium (PEA).  $\text{BA}_2\text{PbI}_4$  is the most studied 2DLP system with an aliphatic chain cation, and  $\text{UDA}_2\text{PbI}_4$  provides insight on the impact of the aliphatic chain length on the optoelectronic properties.  $\text{PEA}_2\text{PbI}_4$  is the archetype of a 2D perovskite with a phenyl ring in the organic portion that leads to different properties of the organic layer, for example in its stiffness. Furthermore, the above materials have different symmetries in their low-temperature phase (here

our structural characterization is in agreement with literature, as discussed in the Supporting Information (SI in Section 1).

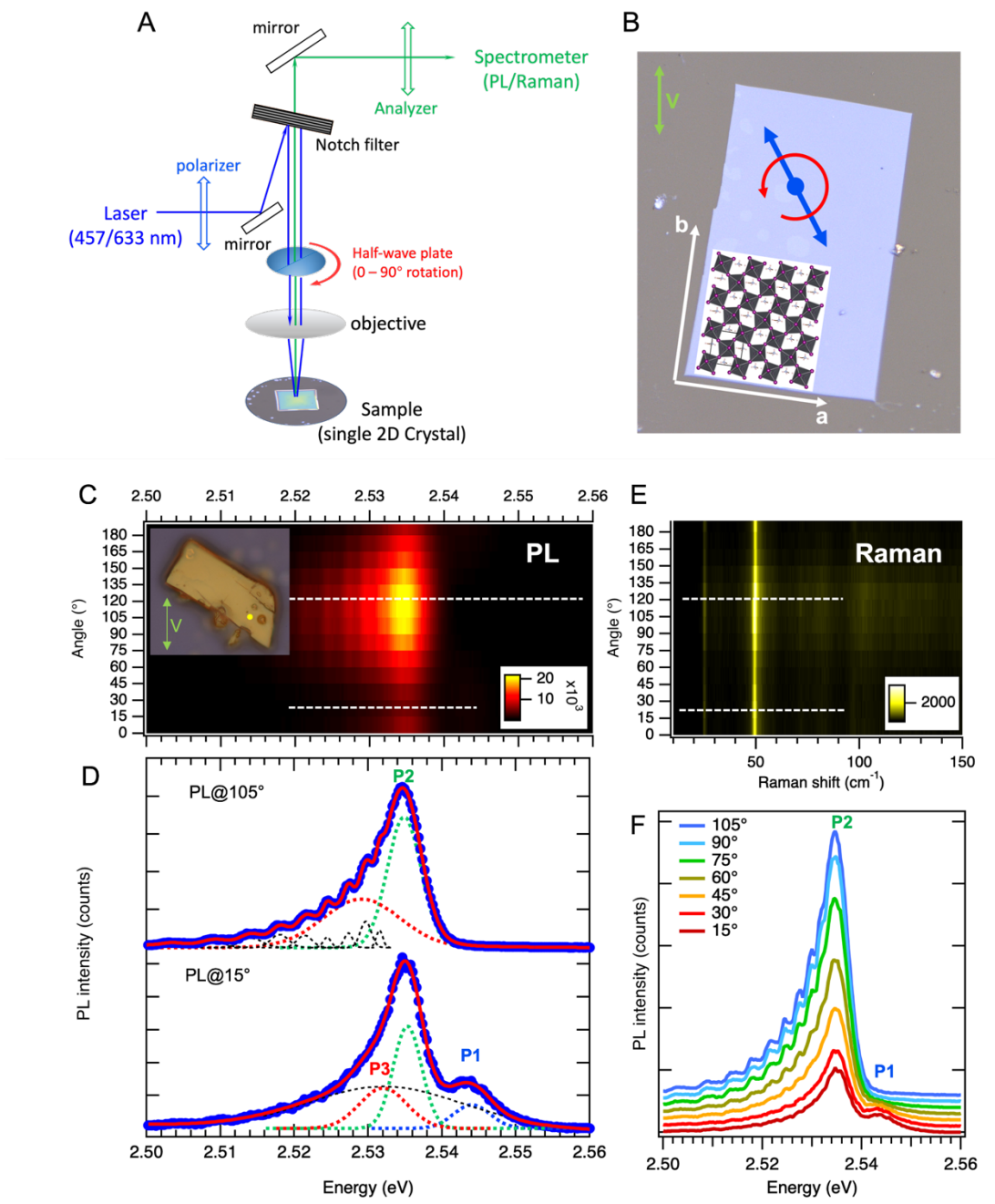


**Figure 1.** Directional photoluminescence and Raman spectra from single 2D perovskite flakes. A) Scheme illustrating the setup for the angle-resolved PL and Raman spectroscopy experiments. The half-

wave plate in both the combined excitation and collection path allows to rotate the angle of the incident linear polarization with respect to the orientation of the exfoliated single crystalline perovskite flake under investigation. PL and Raman spectroscopy measurements were recorded from the same micron-size spot of the 2D perovskite flakes. B) Optical microscope image of a single exfoliated 2D perovskite flake overlaid with an illustration of its octahedra lattice. The blue arrow illustrates the linear polarization impinging on the sample, which is defined by the angle of the half wave plate that can be rotated with respect to the orientation of the flake (red circular arrow) and the vertical axis of the setup (green arrow) that corresponds to the analyzer direction. C) Color map of the angle-dependent PL intensity with laser excitation at 457 nm (2.71 eV). The inset shows an optical image of the measured flake, where the yellow dot shows the location of the excitation spot, and the green arrow indicates the direction of the (fixed) vertical analyzer of the optical setup. D) PL spectra recorded at angles of 15° and 105° (white dashed lines in A) together with Gaussian fitting of the spectra. E) Waterfall plot of the spectra recorded from 15° (red) to 105° (blue), which show the increase of P2 and decrease of P1 with increasing angle. F) Angle-resolved Raman spectra displayed as a color map, recorded with 457 nm laser excitation from the same spot as the PL. See Section 2 in the SI for data from another BA<sub>2</sub>PbI<sub>4</sub> flake.

The angle-resolved PL spectra measured from a single BA<sub>2</sub>PbI<sub>4</sub> flake are shown in Figure 1C. We clearly observe a maximum in the overall emission intensity at an angle of around 105°-120° and a minimum at around 15°. These angles correspond to those of the straight edges of the flake parallel to the vertical direction of the analyzer (see inset), and therefore we can associate the main emission intensity roughly to be along one of the major axes of the octahedra lattice. Gaussian fitting of the emission spectra reveals the contributions of two bands to the main peak, as depicted in Figure 1D, where the spectra recorded at 15° and 105° are displayed. The emission at 105° is characterized by a Gaussian peak (P2) at 2.534 eV with width of 3.5 meV (we take as Gaussian peak width twice the standard deviation) that has a series of small narrow peaks overlaying its

low energy side, which feature a non-equidistant spacing that increases from 1.8 meV to 5 meV towards lower energies. The spectrum at  $15^\circ$  can be well fitted with four Gaussian peaks, three with similar narrow width of around 3 meV, and one broader background peak with 15 meV width. We associate the peaks with ca 3 meV width to the confined band edge excitons, and focus on the peaks labeled P1 and P2 that show an orthogonal behavior in intensity with respect to the polarization angle (Peak P3 has a similar angular behavior as peak P2, as evident in Figure 2C). Fig. 2C shows that P1 decreases from  $15^\circ$  to  $105^\circ$ , while P2 increases. Therefore, we assign P1 and P2 to the confined excitons along the orthogonal in-plane directions of the major axes (respectively  $a$  and  $b$  in Figure 1B) of the 2D single crystal. The resonant Raman spectra recorded from the same region are depicted in Figure 1F. Dominant modes are found at  $25\text{ cm}^{-1}$  and  $49\text{ cm}^{-1}$ , which have their intensity maxima at the same angles as the PL maxima of peaks P1 and P2 (indicated by the white dashed lines in Figure 1C,F). We therefore conclude that these low frequency phonons, which correspond to octahedral twists ( $25\text{ cm}^{-1}$ ) and Pb-I bond bending and stretching ( $49\text{ cm}^{-1}$ ),<sup>22, 26-28</sup> are fundamentally involved in the emission dynamics. To summarize, the regular  $\text{BA}_2\text{PbI}_4$  flake manifests two emission bands, P1 and P2&P3, respectively, that have their intensity maxima at orthogonal angles, and which can be associated to the in-plane confined exciton modes along the major axis of the octahedra lattice. Intensity maxima of the low-frequency phonon modes occur at the same angles as the emission intensity maxima, pointing to a strong impact of electron-phonon coupling with these low-frequency vibrational modes in the recombination dynamics.

We now turn to  $\text{UDA}_2\text{PbI}_4$  that features an organic cation with a longer aliphatic chain (11 carbons), which leads to a thicker organic layer and stronger dielectric confinement. Accordingly, the emission of  $\text{UDA}_2\text{PbI}_4$  is blue-shifted with respect to  $\text{BA}_2\text{PbI}_4$ , as shown in Figure S2 in the SI.

Furthermore, from literature we expect the low temperature crystal phase of  $\text{UDA}_2\text{PbI}_4$  to be monoclinic, with a stronger out-of-plane octahedra tilting.<sup>29</sup>

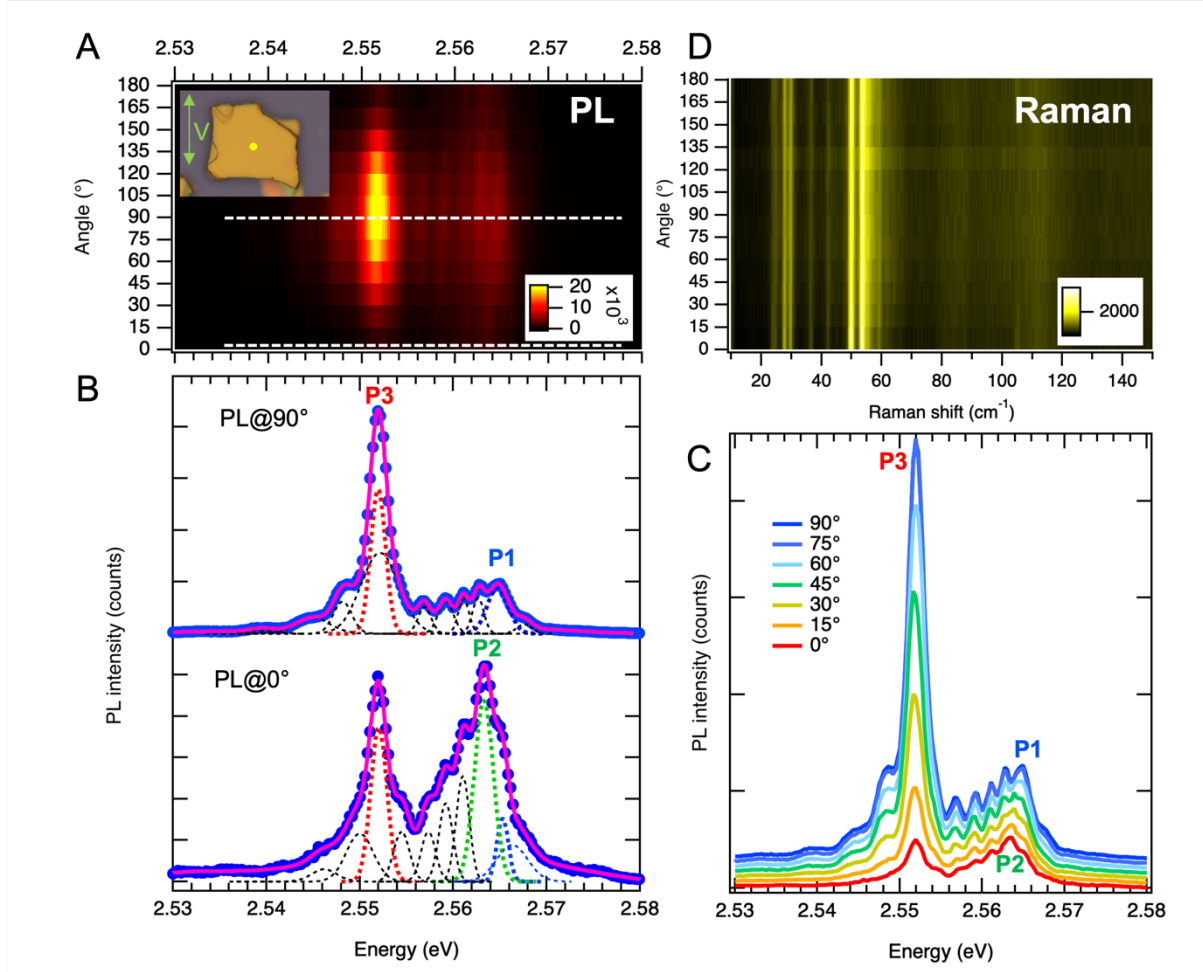


**Figure 2.** Angle-resolved PL and Raman spectra of  $\text{UDA}_2\text{PbI}_4$ . A) Color map of the angle-dependent PL intensity. The inset shows an optical microscope image of the measured flake, the yellow dot illustrates the excitation spot, and the green arrow indicates the direction of the analyzer in the optical setup. B) Normalized PL spectra recorded at angle of 0° and 90° (white dashed lines in A) together with Gaussian fitting. C) Waterfall plot of the spectra recorded from 0° (red) to 90° (blue) - as indicated by the white arrow in A -, which show the dominant increase of P3, and a more rapid increase of P1 with respect to P2 (see Section 3 in the SI for data from another  $\text{UDA}_2\text{PbI}_4$  flake). D) Angle-resolved resonant Raman



spectra recorded with 457 nm excitation from the same spot as the PL spectra, displayed as color map. No distinct angle dependence of the phonon intensities is observed. All spectra were recorded at  $T=4\text{K}$  with excitation at 457 nm.

**Figure 2A-C** displays the angle-resolved PL of a single  $\text{UDA}_2\text{PbI}_4$  flake. In contrast to  $\text{BA}_2\text{PbI}_4$ , all emission peaks in the  $\text{UDA}_2\text{PbI}_4$  spectrum have their intensity maximum at the same angle, at around  $90^\circ$  (Figure 2C). However, we distinguish differences in the strength of the intensity increase with changing angle: peak P1 is weaker than P2 at  $0^\circ$ , which is reversed at  $90^\circ$ , and peak P3 features the strongest angle-dependent increase in intensity. We therefore associate the peaks P1, P2, and P3 to exciton states with different (in-plane) symmetry. The polarization dependence of the emission peaks with a single angular maximum goes along with phonon modes under resonant excitation that manifest no significant angle dependent intensity variation, see Figure 2D, and with vibrations along the diagonal lattice directions (Figure 3), as will be discussed in the following.

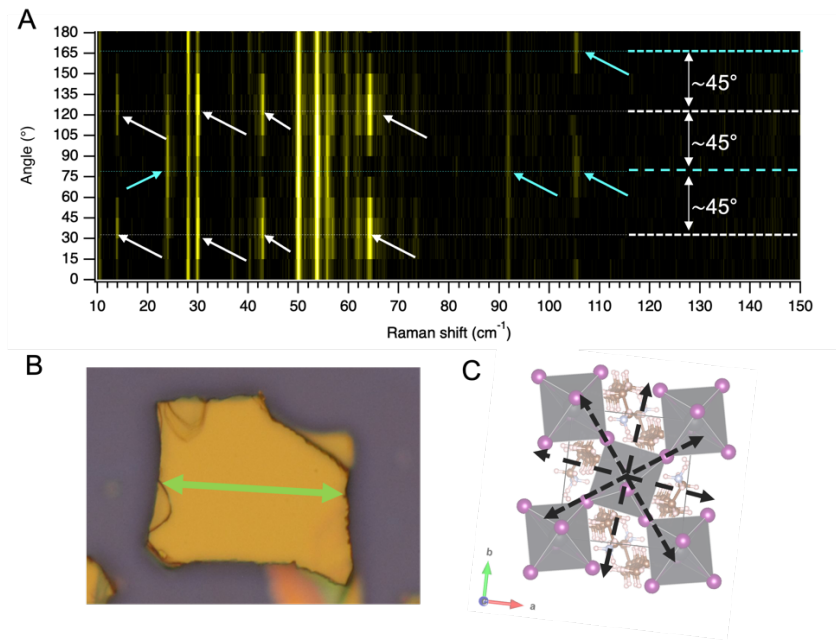


**Figure 3.** A) Angle-resolved non-resonant Raman spectra of  $\text{UDA}_2\text{PbI}_4$  recorded with excitation wavelength of 633 nm (1.96 eV) at  $T=4\text{K}$ . A very rich phonon spectrum is observed, containing a large number of modes that show different angular behavior. White arrows indicate intensity maxima of phonons at angles of  $30^\circ$  and  $120^\circ$ , cyan arrows indicate maxima at  $75^\circ$  and  $165^\circ$ . The  $45^\circ$  difference between these angles evidences phonon modes along the major axes of the octahedra lattice and along their diagonals. B) Optical microscope image of the flake under investigation, the green arrow indicates the polarization direction of strong emission. C) Top view on the crystallographic unit cell for  $\text{DA}_2\text{PbI}_4$  (10 carbons), the in-plane orientation is rotated to match the straight edges of the flake in B, and the dashed lines indicate the directions that correspond to the Raman intensity maxima in A.

Interestingly, we observe a strong directionality of the phonon modes under non-resonant excitation in the Raman spectra of  $\text{UDA}_2\text{PbI}_4$ , as shown in **Figure 3A**. Here we find the intensity maxima of different phonon modes at angles that differ by multiples of  $45^\circ$ , which lifts the orthogonal occurrence of the phonon bands. It is therefore plausible that phonon modes with different directionality are coupled the recombination processes of the confined excitons, which homogenizes the angular intensity dependence of the different emission peaks. In this picture the emission polarization is defined by the vector product of the emission dipoles and the different phonons. As for  $\text{BA}_2\text{PbI}_4$ , we also observe a series of narrow peaks with few meV spacing in the emission spectra of  $\text{UDA}_2\text{PbI}_4$  (Figure 2A-C). This series mainly occurs on the low energy side of peaks P1&P2, and is more dominant at the angle where strong emission occurs.

We also investigated the emission and vibrational properties of single  $\text{PEA}_2\text{PbI}_4$  flakes and report the PL and Raman spectra in Section 4 in the SI. Overall, the behavior of  $\text{PEA}_2\text{PbI}_4$  is similar to that of  $\text{UDA}_2\text{PbI}_4$ , featuring intensity maxima of the emission peaks at a similar polarization angle,

and phonon bands with a strong angular intensity variation under non-resonant excitation in the Raman spectra, while under resonant excitation no significant angular dependence is present. The main emission band shifts in energy with polarization angle, in agreement with literature.<sup>9</sup> Interestingly, in the PL spectra of  $\text{PEA}_2\text{PbI}_4$  we observe two additional strong sharp peaks in the emission spectrum, and their energy spacing of 9.4 meV corresponds very well to the energy of the out-of-plane phonon mode, see Figure S8. Therefore, we conclude that these sharp peaks originate from a vibronic progression related to this out-of-plane phonon mode that is favored by the stiffer organic layer in  $\text{PEA}_2\text{PbI}_4$ , in agreement with literature.<sup>20, 21</sup> This interpretation is corroborated by the weak angular intensity dependence of both the sharp emission peaks and of the out-of-plane phonon mode. We also note two weak double-peak structures that are present at the high energy side of the main emission band that show an orthogonal intensity dependence with respect to their polarization angle: the higher energy double-peak vanishes towards the polarization angle at which all other peaks have their maximum intensity (Figure S9). This could indicate an out-of-plane confined exciton state that is weakly coupled via the tilting of the octahedra.

Summarizing our findings on the correlation of the emission properties with their vibrational behavior we observe the following: The  $\text{BA}_2\text{PbI}_4$  flakes feature relatively few low-frequency phonon modes, with mostly two orthogonal angle-dependent maxima. Accordingly, we observe exciton peaks in the emission of the  $\text{BA}_2\text{PbI}_4$  flakes that have their intensity maximum with polarization along these two directions. For  $\text{UDA}_2\text{PbI}_4$ , where the longer aliphatic chain leads to a larger thickness of the soft organic layers, the vibrational response and the optical behavior are different.  $\text{UDA}_2\text{PbI}_4$  crystals feature a much richer phonon spectrum (best resolved under non-resonant excitation) that contains vibrations along both major axes of the octahedra lattice and, importantly, also along its diagonals. Therefore, the set of phonon modes cannot be separated in

two orthogonal components, and the intensity of all emission bands maximizes at one distinct polarization angle. This goes along with a negligible angle dependence of the phonon modes under resonant excitation, where the scattering is strongly coupled to hot excitons. For  $\text{PEA}_2\text{PbI}_4$ , the higher stiffness of the organic layers (due to the  $\pi - \pi$  bonding of the phenyl rings<sup>30</sup>) leads to significant coupling of the excitons also to out-of-plane phonon modes that have higher frequencies (around 10 meV), and which are isotropic in the octahedra lattice plane, and weak higher energy emission peaks with orthogonal polarization indicate signatures of out-of plane confined excitons. For all studied samples, the dominant presence of the low-frequency phonon modes ( $< 7$  meV) in the resonant (and non-resonant) Raman spectra underpins their important role in the optical recombination processes. This behavior supports the interpretation that polaron vibronic progressions involving these modes with few meV energy are dominant in band edge emission.

**Figure 4** reports temperature dependent PL experiments in the range from 4-80K that reveal how the band edge emission fine structure observed at 4K evolves from a single broad peak at 80K for all samples. The exciton-fine structure emerges in the temperature range below 80K, which underpins the key role of the low-frequency phonons with energy below 10 meV in the emission dynamics. With decreasing temperature, we observe a red shift of the main emission band for  $\text{BA}_2\text{PbI}_4$  (Figure 4A) and  $\text{PEA}_2\text{PbI}_4$  (Figure 4C,D), in agreement with literature,<sup>31, 32</sup> while for  $\text{UDA}_2\text{PbI}_4$  (Figure 4B) the broad peak observed in the range from 60 -80 K splits into a set of sharper peaks below 40K. For the systems build with organic cations with an aliphatic chain ( $\text{BA}_2\text{PbI}_4$  and  $\text{UDA}_2\text{PbI}_4$ ), the emission intensity increases significantly with decreasing temperature. This is different for  $\text{PEA}_2\text{PbI}_4$ , where the emission intensity has a maximum at around 50K, a local minimum at 20K, and then again relatively strong emission intensity at 4K. Such

behavior can be explained by the involvement of phonons with different energies in the emission process, namely the out-of-plane phonon at 9.4 meV ( $77\text{ cm}^{-1}$ ), and the low-frequency in-plane phonons in the range from 2.5 -6 meV ( $20\text{-}50\text{ cm}^{-1}$ ). The weak dependence of the emission intensity at temperatures below 30K for  $\text{PEA}_2\text{PbI}_4$  indicates that the impact of the in-plane phonons to the thermal coupling of the exciton band edge states is much less as compared to  $\text{BA}_2\text{PbI}_4$  and  $\text{UDA}_2\text{PbI}_4$ . Accordingly, we do not find a low-frequency signal in the resonant Raman spectra recorded from the  $\text{PEA}_2\text{PbI}_4$  flake, see Figure S10.

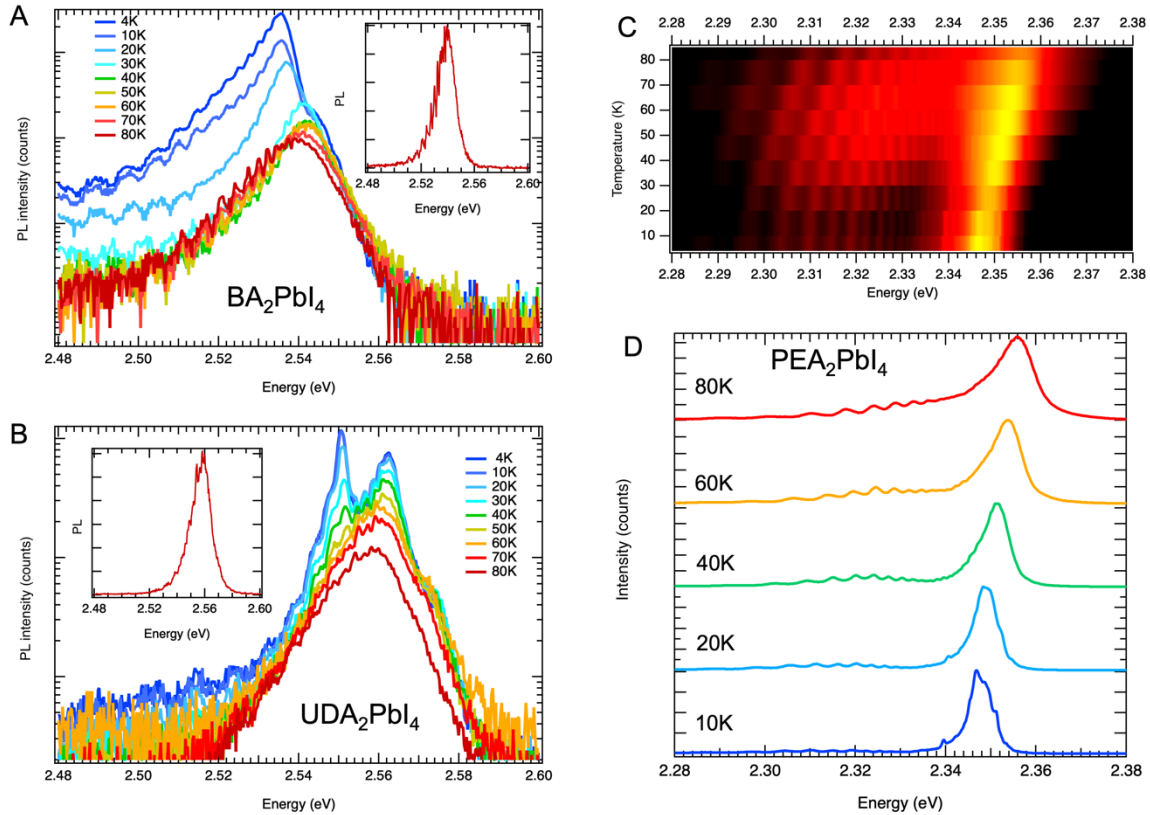


**Figure 4.** Temperature dependence of the band-edge emission of single lead-iodide microcrystals. A-B) Semi-log plot of the emission intensity of  $\text{BA}_2\text{PbI}_4$  (A) and  $\text{UDA}_2\text{PbI}_4$  (B). The insets show the emission at 80K on a linear scale. C-D) Color-plot and emission spectra at different temperatures of a single  $\text{PEA}_2\text{PbI}_4$  flake.

In conclusion, our combined study of the angle-resolved photoluminescence and Raman spectra of single two-dimensional lead-iodide microcrystals evidenced the strong correlation of the low-frequency phonons with the band edge emission. In particular, the exciton polarization is not isotropic in the plane of the octahedra lattice, as would be expected from the electronic structure,<sup>13</sup> highlighting the strong influence of the exciton-phonon coupling. Here subtle differences in the organic cation, like a change in the length of the aliphatic chain, can lead to very different emission polarization and PL line width broadening. Our results reveal the complexity of the electron-phonon coupling and provide detailed insight on how the directionality of the phonons impacts the polarization and intensity of the band-edge emission. One consequence is that the typically applied Bose-Einstein modeling of the thermal broadening of the PL, which is based on a single LO phonon energy,<sup>33,34</sup> is not adequate to describe the thermal behavior of the 2DLPs. In this respect, the correspondence of the energy of the directional low-energy phonons with the thermal range below 80K, where the complex splitting of the band edge emission appears, highlights the impact of multiple low energy phonons on the emission properties of these materials. These insights on how phonon directionality impacts exciton polarization, are important for designing photonic devices, in particular, where the orientation of the emission dipoles is crucial for their performance, for example in optical cavities and other resonators.

## EXPERIMENTAL SECTION

Materials. Lead (II) iodide (PbI<sub>2</sub>, 99 %), hydroiodic acid (HI, 57 %, distilled, 99.999 % trace metal basis), hypophosphorous acid (H<sub>3</sub>PO<sub>2</sub>, 50 %), phenethylamine (PEA, 99 %), undecylamine (UDA, ≥98 %), butylamine (BA, 99.5 %), ethyl acetate (≥99.5 %), toluene (≥99.7 %) were purchased from Sigma-Aldrich without any further purification.

Sample fabrication. Microcrystalline powders of  $\text{BA}_2\text{PbI}_4$ ,  $\text{UDA}_2\text{PbI}_4$  and  $\text{PEA}_2\text{PbI}_4$  were synthesized by a modified antisolvent-assisted fast crystallization approach published previously by our group.<sup>35</sup> Briefly, 0.25 mmol  $\text{PbI}_2$  was dissolved in 200  $\mu\text{l}$  of HI and 108  $\mu\text{l}$  of  $\text{H}_2\text{PO}_3$ , followed by the dilution with 2 ml ethyl acetate for  $\text{UDA}_2\text{PbI}_4$  and  $\text{PEA}_2\text{PbI}_4$  and 2 ml ethyl acetate and 1 ml toluene for  $\text{BA}_2\text{PbI}_4$ . Afterward, 0.6 mmol of the respective amine was directly injected into the mixture, leading to the immediate crystallization of orange microcrystals. The reaction mixture was continuously agitated for at least 3 h. Subsequently, the microcrystalline powder was separated from the solution by centrifugation at 6000 rpm, followed by the redispersion in the respective solvent system. The washing procedure was repeated twice and the purified crystals were dried under vacuum for 1 h.

Angle resolved PL and Raman experiments. Raman experiments were performed under resonant conditions with wavelengths of 457 nm from an  $\text{Ar}^+$  laser and non-resonant conditions with wavelengths of 633 nm from a He–Ne laser. The spectra were collected in a backscattering geometry using a Jobin–Yvon HR800 micro-Raman system equipped with a charged-coupled detector (CCD) and a 50 $\times$  objective (numerical aperture (NA) of 0.55) with a long working distance. 2400 lines/mm gratings were used yielding a spectral resolution was 0.19  $\text{cm}^{-1}$  per CCD pixel under 633 nm excitation with 2400 lines/mm. The laser plasma lines were removed by Bragg-volume-grating-based bandpass filters (BPF) from OptiGrate Corp. The samples were placed in a closed cycle cryostat (Montana Instruments) and cooled to cryogenic temperatures of about 4K. For angle-resolved Raman measurements, two vertical polarizers and one rotational half-wave plate were utilized. One polarizer was inserted in the incident path, and one analyzer with polarization parallel was allocated in the scattered path before the spectrometer. The half-wave plate was positioned in the common optical path of the incident and scattered light to

simultaneously alter their polarization directions. Rotating the fast axis of the half-wave plate by an angle of  $\varphi/2$  is equivalent to a rotation of the sample by an angle of  $\varphi$  relative to the polarization directions of the polarizer and analyzer.<sup>36</sup> The laser power was kept lower than 40  $\mu\text{W}$  to avoid laser-induced degradation of the sample. For the temperature-dependent measurements, the sample was first cooled to 4 K and then the temperature was raised stepwise to the indicated values. The angle-resolved photoluminescence spectra were recorded with the Raman setup using a grating with 600 lines/mm and a laser at 457 nm wavelength from an Ar<sup>+</sup> laser. For PL measurements, the laser power is lower than 0.1  $\mu\text{W}$ .

## ASSOCIATED CONTENT

**Supporting Information.** The following files are available free of charge.

The Supporting\_Information.pdf file contains:

- Structural properties of the 2DLPs under discussion
- Additional Raman and PL Data from BA<sub>2</sub>PbI<sub>4</sub> flakes
- Additional Raman and PL Data from UDA<sub>2</sub>PbI<sub>4</sub> flakes
- Angle-resolved emission and Raman spectra of PEA<sub>2</sub>PbI<sub>4</sub>

## AUTHOR INFORMATION

### Corresponding Author

\* Roman.krahne@iit.it



## Author Contributions

The manuscript was written through contributions of all authors. All authors have given approval to the final version of the manuscript.

## ACKNOWLEDGMENT

A. S. acknowledges the European Union's Horizon 2020 research and innovation programme under the Marie Skłodowska-Curie Funding Program (Project Together, grant agreement No.101067869). R.K acknowledges funding by the European Union under Project 101131111 – DELIGHT. P.H. and M.L. acknowledge the support from National Natural Science Foundation of China (Grant Nos. 12322401 and 12127807), Beijing Nova Program (Grant No. 20230484301), Youth Innovation Promotion Association, Chinese Academy of Sciences (No. 2023125).

## REFERENCES

1. Smith, M. D.; Crace, E. J.; Jaffe, A.; Karunadasa, H. I. The Diversity of Layered Halide Perovskites, *Annu. Rev. Mater. Res.* **2018**, 48, 111-136.
2. Tanaka, K.; Takahashi, T.; Kondo, T.; Umeda, K.; Ema, K.; Umebayashi, T.; Asai, K.; Uchida, K.; Miura, N. Electronic and Excitonic Structures of Inorganic–Organic Perovskite-Type Quantum-Well Crystal (C<sub>4</sub>H<sub>9</sub>NH<sub>3</sub>)<sub>2</sub>PbBr<sub>4</sub>, *Jap. J. Appl. Phys.* **2005**, 44, 5923.
3. Blancon, J. C.; Stier, A. V.; Tsai, H.; Nie, W.; Stoumpos, C. C.; Traoré, B.; Pedesseau, L.; Kepenekian, M.; Katsutani, F.; Noe, G. T.; Kono, J.; Tretiak, S.; Crooker, S. A.; Katan, C.; Kanatzidis, M. G.; Crochet, J. J.; Even, J.; Mohite, A. D. Scaling Law for Excitons in 2D Perovskite Quantum Wells, *Nat. Commun.* **2018**, 9, 2254.
4. Mauck, C. M.; Tisdale, W. A. Excitons in 2D Organic–Inorganic Halide Perovskites, *Trends Chem.* **2019**, 1, 380-393.
5. Cho, Y.; Berkelbach, T. C. Optical Properties of Layered Hybrid Organic–Inorganic Halide Perovskites: A Tight-Binding GW-BSE Study, *J. Phys. Chem. Lett.* **2019**, 10, 6189-6196.
6. Li, X.; Hoffman, J. M.; Kanatzidis, M. G. The 2D Halide Perovskite Rulebook: How the Spacer Influences Everything from the Structure to Optoelectronic Device Efficiency, *Chem. Rev.* **2021**, 121, 2230-2291.
7. Smith, M. D.; Karunadasa, H. I. White-Light Emission from Layered Halide Perovskites, *Acc. Chem. Res.* **2018**, 51, 619-627.
8. Dhanabalan, B.; Biffi, G.; Moliterni, A.; Olieric, V.; Giannini, C.; Saleh, G.; Ponet, L.; Prato, M.; Imran, M.; Manna, L.; Krahne, R.; Artyukhin, S.; Arciniegas, M. P. Engineering the

- Optical Emission and Robustness of Metal-Halide Layered Perovskites through Ligand Accommodation, *Adv. Mater.* **2021**, 33, 2008004.
9. Do, T. T. H.; Granados del Águila, A.; Zhang, D.; Xing, J.; Liu, S.; Prosnikov, M. A.; Gao, W.; Chang, K.; Christianen, P. C. M.; Xiong, Q. Bright Exciton Fine-Structure in Two-Dimensional Lead Halide Perovskites, *Nano Lett.* **2020**, 20, 5141-5148.
  10. Dyksik, M.; Duim, H.; Maude, D. K.; Baranowski, M.; Loi, M. A.; Plochocka, P. Brightening of Dark Excitons in 2D Perovskites, *Sci. Adv.* **2021**, 7, eabk0904.
  11. Quarti, C.; Giorgi, G.; Katan, C.; Even, J.; Palummo, M. Exciton Ground State Fine Structure and Excited States Landscape in Layered Halide Perovskites from Combined BSE Simulations and Symmetry Analysis, *Adv. Opt. Mater.* **2023**, n/a, 2202801.
  12. Ammirati, G.; Martelli, F.; O'Keeffe, P.; Turchini, S.; Paladini, A.; Palummo, M.; Giorgi, G.; Cinquino, M.; De Giorgi, M.; De Marco, L.; Catone, D. Band Structure and Exciton Dynamics in Quasi-2D Dodecylammonium Halide Perovskites, *Adv. Opt. Mater.* **2023**, 11, 2201874.
  13. Giorgi, G.; Yamashita, K.; Palummo, M. Nature of the Electronic and Optical Excitations of Ruddlesden–Popper Hybrid Organic–Inorganic Perovskites: The Role of the Many-Body Interactions, *J. Phys. Chem. Lett.* **2018**, 9, 5891-5896.
  14. Katan, C.; Mercier, N.; Even, J. Quantum and Dielectric Confinement Effects in Lower-Dimensional Hybrid Perovskite Semiconductors, *Chem. Rev.* **2019**, 119, 3140-3192.
  15. Sercel, P. C.; Efros, A. L. Unique Signatures of the Rashba Effect in the Magneto-Optical Properties of Two-Dimensional Semiconductors, *Phys. Rev. B* **2023**, 107, 195436.
  16. Shinde, A.; Rajput, P. K.; Makhija, U.; Tanwar, R.; Mandal, P.; Nag, A. Emissive Dark Excitons in Monoclinic Two-Dimensional Hybrid Lead Iodide Perovskites, *Nano Lett.* **2023**, 23, 6985-6993.
  17. Folpini, G.; Cortecchia, D.; Petrozza, A.; Srimath Kandada, A. R. The Role of a Dark Exciton Reservoir in the Luminescence Efficiency of Two-Dimensional Tin Iodide Perovskites, *J. Mater. Chem. C* **2020**, 8, 10889-10896.
  18. Posmyk, K.; Dyksik, M.; Surrente, A.; Maude, D. K.; Zawadzka, N.; Babiński, A.; Molas, M. R.; Paritmongkol, W.; Mączka, M.; Tisdale, W. A.; Plochocka, P.; Baranowski, M. Exciton Fine Structure in 2D Perovskites: The out-of-Plane Excitonic State, *Adv. Opt. Mater.* **2023**, 2300877.
  19. Straus, D. B.; Kagan, C. R. Photophysics of Two-Dimensional Semiconducting Organic–Inorganic Metal-Halide Perovskites, *Annu. Rev. Phys. Chem.* **2022**, 73, 403-428.
  20. Straus, D. B.; Hurtado Parra, S.; Iotov, N.; Zhao, Q.; Gau, M. R.; Carroll, P. J.; Kikkawa, J. M.; Kagan, C. R. Tailoring Hot Exciton Dynamics in 2D Hybrid Perovskites through Cation Modification, *ACS Nano* **2020**, 14, 3621-3629.
  21. Straus, D. B.; Hurtado Parra, S.; Iotov, N.; Gebhardt, J.; Rappe, A. M.; Subotnik, J. E.; Kikkawa, J. M.; Kagan, C. R. Direct Observation of Electron–Phonon Coupling and Slow Vibrational Relaxation in Organic–Inorganic Hybrid Perovskites, *J. Am. Chem. Soc.* **2016**, 138, 13798-13801.
  22. Thouin, F.; Valverde-Chávez, D. A.; Quarti, C.; Cortecchia, D.; Bargigia, I.; Beljonne, D.; Petrozza, A.; Silva, C.; Srimath Kandada, A. R. Phonon Coherences Reveal the Polaronic Character of Excitons in Two-Dimensional Lead Halide Perovskites, *Nat. Mater.* **2019**, 18, 349-356.
  23. Thouin, F.; Srimath Kandada, A. R.; Valverde-Chávez, D. A.; Cortecchia, D.; Bargigia, I.; Petrozza, A.; Yang, X.; Bittner, E. R.; Silva, C. Electron–Phonon Couplings Inherent in

- Polarons Drive Exciton Dynamics in Two-Dimensional Metal-Halide Perovskites, *Chem. Mater.* **2019**, 31, 7085-7091.
24. Srimath Kandada, A. R.; Silva, C. Exciton Polarons in Two-Dimensional Hybrid Metal-Halide Perovskites, *J. Phys. Chem. Lett.* **2020**, 11, 3173-3184.
  25. Dyksik, M.; Beret, D.; Baranowski, M.; Duim, H.; Moyano, S.; Posmyk, K.; Mlayah, A.; Adjokatse, S.; Maude, D. K.; Loi, M. A.; Puech, P.; Plochocka, P. Polaron Vibronic Progression Shapes the Optical Response of 2D Perovskites, *Adv. Science* **2023**, 2305182.
  26. Pérez-Osorio, M. A.; Lin, Q.; Phillips, R. T.; Milot, R. L.; Herz, L. M.; Johnston, M. B.; Giustino, F. Raman Spectrum of the Organic–Inorganic Halide Perovskite CH<sub>3</sub>NH<sub>3</sub>PbI<sub>3</sub> from First Principles and High-Resolution Low-Temperature Raman Measurements, *J. Phys. Chem. C* **2018**, 122, 21703-21717.
  27. Pérez-Osorio, M. A.; Milot, R. L.; Filip, M. R.; Patel, J. B.; Herz, L. M.; Johnston, M. B.; Giustino, F. Vibrational Properties of the Organic–Inorganic Halide Perovskite CH<sub>3</sub>NH<sub>3</sub>PbI<sub>3</sub> from Theory and Experiment: Factor Group Analysis, First-Principles Calculations, and Low-Temperature Infrared Spectra, *J. Phys. Chem. C* **2015**, 119, 25703-25718.
  28. Lin, M.-L.; Dhanabalan, B.; Biffi, G.; Leng, Y.-C.; Kutkan, S.; Arciniegas, M. P.; Tan, P.-H.; Krahne, R. Correlating Symmetries of Low-Frequency Vibrations and Self-Trapped Excitons in Layered Perovskites for Light Emission with Different Colors, *Small* **2022**, 18, 2106759.
  29. Lemmerer, A.; Billing, D. G. Synthesis, Characterization and Phase Transitions of the Inorganic–Organic Layered Perovskite-Type Hybrids [(CNH<sub>2n+1</sub>NH<sub>3</sub>)<sub>2</sub>PbI<sub>4</sub>], N = 7, 8, 9 and 10, *Dalton Trans.* **2012**, 41, 1146-1157.
  30. Tu, Q.; Spanopoulos, I.; Vasileiadou, E. S.; Li, X.; Kanatzidis, M. G.; Shekhawat, G. S.; Dravid, V. P. Exploring the Factors Affecting the Mechanical Properties of 2D Hybrid Organic–Inorganic Perovskites, *ACS Appl. Mater. & Interfaces* **2020**, 12, 20440-20447.
  31. Gan, L.; Li, J.; Fang, Z.; He, H.; Ye, Z. Effects of Organic Cation Length on Exciton Recombination in Two-Dimensional Layered Lead Iodide Hybrid Perovskite Crystals, *J. Phys. Chem. Lett.* **2017**, 8, 5177-5183.
  32. Kahmann, S.; Duim, H.; Fang, H.-H.; Dyksik, M.; Adjokatse, S.; Rivera Medina, M.; Pitaro, M.; Plochocka, P.; Loi, M. A. Photophysics of Two-Dimensional Perovskites—Learning from Metal Halide Substitution, *Adv. Funct. Mater.* **2021**, 31, 2103778.
  33. Wright, A. D.; Verdi, C.; Milot, R. L.; Eperon, G. E.; Pérez-Osorio, M. A.; Snaith, H. J.; Giustino, F.; Johnston, M. B.; Herz, L. M. Electron-Phonon Coupling in Hybrid Lead Halide Perovskites, *Nat. Commun.* **2016**, 7, 1-9.
  34. Kutkan, S.; Dhanabalan, B.; Lin, M.-L.; Tan, P.-H.; Schleusener, A.; Arciniegas, M. P.; Krahne, R. Impact of the Organic Cation on the Band-Edge Emission of Two-Dimensional Lead–Bromide Perovskites, *Nanoscale* **2023**, 15, 12880-12888.
  35. Dhanabalan, B.; Castelli, A.; Palei, M.; Spirito, D.; Manna, L.; Krahne, R.; Arciniegas, M. Simple Fabrication of Layered Halide Perovskite Platelets and Enhanced Photoluminescence from Mechanically Exfoliated Flakes, *Nanoscale* **2019**, 11, 8334-8342.
  36. Liu, X.-L.; Zhang, X.; Lin, M.-L.; Tan, P.-H. Different Angle-Resolved Polarization Configurations of Raman Spectroscopy: A Case on the Basal and Edge Plane of Two-Dimensional Materials, *Chin. Phys. B* **2017**, 26, 067802.

TOC image

